Matter and Radiation at Extremes | RESEARCH ARTICLE | scitation.org/journal/mre

Optimization of a laser plasma-based x-ray source according to WDM absorption spectroscopy requirements

Cite as: Matter Radiat. Extremes 6, 014405 (2021); doi: 10.1063/5.0025646
Submitted: 18 August 2020 • Accepted: 20 November 2020 •
Published Online: 24 December 2020

A. S. Martynenko,[1,a] S. A. Pikuz,[1,2,a] I. Yu. Skobelev,[1,2] S. N. Ryazantsev,[1,2] C. D. Baird,[3] N. Booth,[4] L. N. K. Döhl,[3] P. Durey,[3] A. Ya. Faenov,[1,5] D. Farley,[3] R. Kodama,[5,6] K. Lancaster,[3] P. McKenna,[7] C. D. Murphy,[3] C. Spindloe,[4] T. A. Pikuz,[1,5] and N. Woolsey[3]

AFFILIATIONS

[1]Joint Institute for High Temperatures of the Russian Academy of Sciences, 125412 Moscow, Russia
[2]National Research Nuclear University MEPhI, Kashirskoe Sh. 31, 115409 Moscow, Russia
[3]York Plasma Institute, Department of Physics, University of York, York YO10 5DD, United Kingdom
[4]Central Laser Facility, STFC Rutherford Appleton Laboratory, Didcot OX11 0QX, United Kingdom
[5]Open and Transdisciplinary Research Initiative, Osaka University, Osaka 565-0871, Japan
[6]Institute of Laser Engineering, Osaka University, Suita 565-0871, Japan
[7]Department of Physics, SUPA, University of Strathclyde, Glasgow G4 0NG, United Kingdom

Note: This paper is part of the Special Issue on Matter in extreme states created by laser.
[a]**Authors to whom correspondence should be addressed:** artmarty@mail.ru and spikuz@gmail.com

ABSTRACT

X-ray absorption spectroscopy is a well-accepted diagnostic for experimental studies of warm dense matter. It requires a short-lived X-ray source of sufficiently high emissivity and without characteristic lines in the spectral range of interest. In the present work, we discuss how to choose an optimum material and thickness to get a bright source in the wavelength range 2 Å–6 Å (~2 keV to 6 keV) by considering relatively low-Z elements. We demonstrate that the highest emissivity of solid aluminum and silicon foil targets irradiated with a 1-ps high-contrast sub-kJ laser pulse is achieved when the target thickness is close to 10 μm. An outer plastic layer can increase the emissivity even further.

I. INTRODUCTION

X-ray spectroscopy is an experimental tool that enables the determination of the temperature, density, charge state, interionic electromagnetic fields, X-ray emissivity, and transport properties of hot and dense plasmas created by intense lasers (e.g., Refs. 1–3). X-ray emission spectroscopy relies on the creation of highly excited states that form at the high temperature of the plasma. These temperatures typically exceed several hundreds of eV. When a plasma is cool, its X-ray emissivity is low, which prevents the recording and reliable analysis of the emission spectra. X-ray absorption spectroscopy (XAS)[4] is a powerful and practical alternative for cool plasmas. XAS has been used to study laser-induced plasmas,[2,5–8] shock-wave compressed matter,[8–13] and matter heated by X-rays.[8,14–16] Recent attention has focused on using XAS to study warm dense matter (WDM).[17–20] Measurements have been used to validate numerical descriptions of the transport properties of WDM.[2] Understanding transport in WDM is important for fast and shock ignition in laser fusion experiments[21,22] and planetary science.[23,24]

A successful experimental implementation of XAS requires an X-ray source (XRS) that satisfies several important criteria: (1) the source should be sufficiently intense to dominate any self-radiation and have a good signal-to-noise ratio, (2) the emission duration should be sufficiently short to enable time-resolved measurements, and (3) the source should provide an adequate spatial resolution. In general, these three criteria should be met across the spectral range of interest. With sufficient temporal resolution, it is possible to capture "freeze-frame" transient processes, and multiple shots enable frame-by-frame "scans" of evolving systems. Examples of these approaches

are discussed in Refs. 5 and 25. These three criteria can be satisfied with suitably designed relativistic laser-plasma XRS set-ups[26–28] that have X-ray emission duration <0.1 ns, a small size (<5 μm), and a high emissivity across a broad spectral range. However, the specific experimental XRS parameters depend on the individual experimental conditions and requirements. For example, consider a 10-μm-thick Sc foil as the studied target and with a K-edge of around 2.76 Å or 4.5 keV. Its X-ray absorption in the range 2.5 Å–2.75 Å is about 0.9. Therefore, to get an XRS signal with emissivity after absorption that is approximately a factor of 10 higher than the target self-emission, the XRS emissivity prior to absorption has to be hundreds of times higher than the target self-emission.

The lifetime of the XRS plasma should be much shorter than the evolution time of the WDM state. Plasmas generated in solids by a high-contrast ps-short pulse laser are the most suitable. Usually, accurate estimations of XRS plasma lifetimes require comprehensive modeling, yet this is not always necessary. A recombination continuum is emitted until the plasma cools down and recombines, so that is loses its He-like states. Cooling occurs mainly due to adiabatic expansion of the plasma. The lifetime of a plasma depends on its initial size and expansion velocity. The expansion time of a relatively small XRS plasma is orders of magnitude shorter than the expansion of the massive main WDM target, i.e., tens of ps compared to ns.

It would be useful to obtain time-resolved data for an X-ray absorption near-edge structure (XANES). However, no schemes implementing a streak detector and laser-plasma-based XRS have yet been realized, likely due to the insufficient emissivity of the laser. Instead, time-resolved XANES data have been obtained using a CCD detector in multiple-shot mode by scanning the delay between the heating and backlighting laser pulses.[29–31] Alternative forms of XRS used for absorption spectroscopy includes X- and Z-pinches, which provide bright and short-duration emission,[15,32,33] X-ray free-electron lasers (XFELs),[34] laser wakefields,[35–39] and synchrotron sources.[19] These pinch-based sources can be emissivity limited, have pulse durations of more than tens of ns,[17,30] and have reasonable spatial resolution. An XFEL is an exceptional radiation source, providing extraordinarily bright beams of short-duration X-rays with high spatial resolution. Unfortunately, there is limited access to XFEL sources, and this will likely remain so for the foreseeable future. Although solid foils remain the most common XRS targets for XAS in experiments with optical lasers,[5,40–42] other target types include gas jets,[43] clusters, and sophisticated targets.[44–46]

XAS is more complex than self-emission spectroscopy as the technique requires at least two measurements to provide the initial XRS emission spectrum: one before the sample and then one of the X-ray spectrum once it has passed through the sample. An XAS spectrum is extracted by removing the initial XRS spectrum from the transmitted spectrum. Usually these measurements are taken on the same shot, and if different instruments are used to acquire the two measurements, a cross-calibration of the spectrometers and detectors and detailed knowledge of the angular emission of the XRS is necessary. However, recording the XRS emission on each shot eliminates the need to compare with a reference spectrum and therefore reduces the need for reproducibility of the XRS spectrum from shot to shot. Plasma XRS spectra may contain characteristic lines as well as continuum emission of free–free (bremsstrahlung) or bound–free (photorecombination) transitions. Ideally, the XRS spectrum is a featureless continuum, although this is not obligatory. Characteristic lines, such as resonance lines from a K-shell spectrum, are bright and, as such, are often used in imaging. If these lines are present in XAS, it is necessary to ensure the spectral calibration is several times smaller than the width of these spectra features, i.e., of the order of mA. A more robust approach is to choose the backlighting target material in an effort to avoid spectral features across the spectral range of interest.

In this paper, we discuss the optimization of a laser-plasma-based XRS for absorption spectroscopy in the wavelength range of about 2 Å–6 Å (2 keV–6 keV) by considering the merits of different materials and targets of different thickness. We show that targets made of materials of low atomic number, such as aluminum, silicon, phosphorus, sulfur, and potassium, which have atomic numbers $Z = 13, 14, 15, 16$, and 19, respectively, and specific thicknesses are well suited for this purpose.

Detailed modeling of laser-plasma radiation, in general, requires an understanding of the dependencies of its macroscopic parameters on time. First, one needs to know the electron density and temperature, since these parameters determine the photorecombination rate and the populations of ion ground states.

II. CALCULATED EMISSION SPECTRA OF X-RAY SOURCES FOR A SOLID-DENSITY LASER PLASMA

A continuum XRS, i.e., one dominated by bremsstrahlung or recombination emission without spectral lines, is superior for XAS. However, as typical experimental laser-plasma temperatures are noticeably lower than 1 keV, the peak of the bremsstrahlung emission lies in spectral regions of long wavelength or low photon energy (e.g., ~12.35 Å or 1 keV for a plasma temperature of 0.5 keV). In comparison, as photorecombination emission occurs at rather short wavelengths (discussed below), photorecombination can be used to create a continuum XRS in the rather short wavelength or hard X-ray region.

Maximizing the average ionization state requires high plasma densities and temperatures. The rates of collisional ionization are a maximum at temperatures $T_m \approx (0.15–0.3) \times I_p$ and then decrease (I_p is the ionization potential). The ionization rate increases monotonically with increasing plasma density. Therefore, high plasma densities are needed for a harder XRS. Near solid-density plasmas can be created in high-intensity short laser–solid interactions when the laser contrast is sufficiently high; see, for example, Refs. 47–51. Even higher densities can be reached with buried or layered targets. Here an outer transparent coating temporarily prevents the expansion of the XRS emission layer and is discussed in Refs. 52–56.

To estimate the emission spectra for elements with atomic numbers Z = 13–16, we used the atomic radiative-collision kinetic code PrismSPECT[57,58] for the steady state. We assumed that the plasma density is close to that of the solid state and that the long plasma confinement time is sufficient. Chlorine is a gas under normal conditions, whereas potassium exists in compounds only. Therefore, compounds sodium chloride and potassium chloride were used instead of pure sulfur and potassium, respectively. The dense plasma ionization potential depression[59,60] follows the description by Hummer and Mihalas.[61] The results are shown in Fig. 1. These spectra include the bremsstrahlung and recombination emission but exclude the spectral lines. This improves the visualization of the photorecombination continuum profiles, which extend to wavelengths

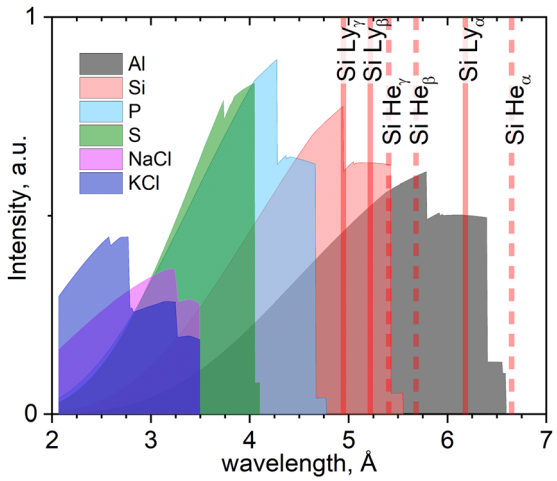

FIG. 1. Comparison of numerical photorecombination continuum emission spectra for a set of elements with atomic numbers Z = 13–16 and compounds sodium chloride and potassium chloride. Aluminum: grey polygon. Silicon: red. Phosphorus: blue. Sulfur: green. Sodium chloride: purple. Potassium chloride: violet. The positions of a few characteristic silicon lines of the resonance series of Ly-like Si (Si XIV, vertical solid lines in the figure) and He-like Si (Si XIII, vertical dashed lines) ions are indicated for clarity. The plasma parameters for each element were chosen individually (Table I). The ion densities n_i were set to be equal to the solid density of the corresponding materials, whereas the electron density and temperature, n_e and T_e, were set to have a fixed sum: $n_eT_e + \sum N_kI_k$.

much shorter than the resonance spectral line positions. This is illustrated for silicon, as the Si XIV (Ly-like) and Si XIII (He-like) resonance line positions are indicated by vertical solid and dashed lines, respectively.

In the calculations, to enable a comparison between different materials and account for different electron configurations and ionization potentials, we simplified how to choose the conditions for our kinetic simulation by ensuring that the sum $n_eT_e + \sum N_kI_k n_eT_e + \sum N_kI_k = 5 \times 10^{26}$ eV/cm^3. Here, n_e and T_e are the electron density and temperature, respectively, N_k is the density of ions with a charge k, and I_k is the energy required for ionization of an atom to a state k, with $n_e = \sum kN_k$. The ion densities, which depend on the solid-state density, electron density, and electron temperature, are given in Table I for each element. This condition assumes that a fixed laser energy will be deposited into targets of different materials. The energy is expended on ionization and heating the plasma up to T_e.

Figure 1 illustrates that the photorecombination continuum peak intensity is roughly the same for each element and can be used to choose the appropriate XRSs for various wavelength ranges. For example, aluminum is best for range 5 Å–5.7 Å, silicon appears to be appropriate across the spectral range 4.25–5 Å, whereas phosphorus is suitable for range 3.75 Å–4.25 Å. Note that the high T_e for potassium (Table I) is due to the solid density whilst maintaining $n_eT_e + \sum N_kI_k = 5 \times 10^{26}$ eV/cm^3.

The results shown in Fig. 1 overestimate the emissivity of XRSs, as in a typical experiment, the ionization states evolve and the plasma expands. The result is that the plasma density averaged over the emission life of the plasma will be lower than that for the solid state. In our modeling, we used plasma temperatures of at least a few hundreds of eV, which ensured the plasmas had high fractions of H- and He-like ions. High temperatures are both relatively easy to achieve using modern laser facilities and desirable because they ensure high peak luminosities in the PCE (photorecombination edge) regions.

III. EXPERIMENTAL OPTIMIZATION OF THE CONFIGURATION OF THE X-RAY SOURCE TARGET

The possibility of using numerical spectra, such as those in Fig. 1, to select an appropriate material for a continuum XRS source was checked by comparing them with experimental measurements of solid foil silicon and aluminum targets irradiated with high-contrast picosecond-duration high-energy laser pulses.

The experiment was conducted with the Vulcan petawatt laser at the Rutherford Appleton Laboratory, UK.[62] This is a Nd:glass laser operating at a wavelength of 1054 nm and uses optical parametric chirped-pulse amplification (OPCPA)[63] to achieve a high laser-to-prepulse contrast. The beam contrast was improved by placing a plasma mirror[64,65] between the focusing f/3 off-axis parabola mirror and the target. This ensured that the laser contrast exceeded 10^{10} at 1 ns.[66] A p-polarized laser pulse was incident on the target at 45° and delivered ~300 J in ~1 ps into a ~7-μm-diameter focal spot. This spot contained 30% of the laser energy, giving an on-target power and intensity of about 0.3 PW and 3×10^{20} W/cm^2. The experimental setup in Fig. 2 shows the position of the parabola, plasma mirror, target, and three X-ray spectrometers.

The following targets were used: (1) silicon foils with thicknesses from 0.5 μm to 30 μm, (2) aluminum foils with thicknesses from 5 μm to 25 μm, and (3) 2-μm silicon foils coated with 1.4 μm CH plastic on both front and rear sides. This plastic coating is transparent to the early part of the high-contrast laser pulse. The inertia of this coating

TABLE I. Ion density n_i, electron density n_e, and electron temperature T_e, which determine the emission spectra in Fig. 2. The indicated PCEs of NaCl correspond to Cl only, whereas the PCEs of KCl correspond to K.

Element or compound	Z	$n_i \times 10^{22}$ (ions/cm^3)	$n_e \times 10^{23}$ (electrons/cm^3)	T_e (eV)	Mean charge	PCE of H-like ion (Å)	PCE of He-like ion (Å)
Al	13	6	6.9	430	11.5	5.61	6.18
Si	14	5	6.2	480	12.4	4.84	5.31
P	15	3.5	4.9	625	14	4.21	4.59
S	16	3.9	5.5	550	14.1	3.66	3.96
NaCl		2.2	3	1150	13.3	3.25	3.5
KCl		1.6	2.7	1255	16.5	2.58	2.77

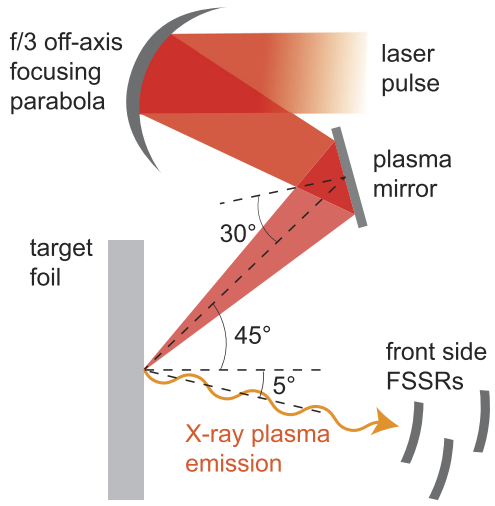

FIG. 2. Top view of the experimental scheme. A solid target is irradiated by a p-polarized laser beam reflected from a focusing parabola and a plasma mirror. The front-side spectrometers are in the plane of the laser beam.

helps prevent expansion of the buried layer until the arrival of the main laser pulse. This is discussed in Refs. 52–55 and the laser interaction with near-solid-density matter in Ref. 56.

Three focusing spectrometers with spatial resolution (FSSRs)[67,68] based on spherically bent crystals were used to record the plasma emission from the front of the target. These were the main diagnostics. Their spectral ranges partially overlapped to allow the cross-calibration of the measurements and the observation of the X-ray spectra across a broad continuous spectral range. This spectral range extends from 4.5 Å to 7.5 Å. The experimental design is described in more detail in Ref. 2. All the spectral measurements were made in space- and time-integrated mode. This broad spectral range enables the bremsstrahlung radiation to be easily distinguishable in the spectra.

Figure 3 compares an experimental space- and time-integrated emission spectrum from a 2-μm silicon foil (indicated with a grey solid curve) with a best-fit model spectrum from PrismSPECT, which is the sum of the characteristic, photorecombination, and bremsstrahlung emissions (indicated with a red solid curve). The blue dashed curve indicates the bremsstrahlung contribution for a plasma. This was based on a single-temperature approximation, with a temperature of T_{Br} = 125 eV. It was estimated from the experimental spectrum between 7 Å and 7.5 Å. This comparison of the experimental and calculated spectra reveals that the ion and electron densities, plasma temperatures, and thicknesses were 2.8 × 10^{22} ion/cm^3, 3.6 × 10^{23} electron/cm^3, 530 eV, and 3 μm, respectively. These values were found by analyzing the broadening of the spectral lines due to the Stark effect and relative intensities of the Si XIV (Si^{13+}) Ly$_\alpha$ and Ly$_\beta$ and Si XIII (Si^{12+}) He$_\alpha$ and He$_\beta$ resonance lines. This type of analysis is described in Ref. 56. The calculated spectrum was extended to 2 Å to highlight the photorecombination contribution to the spectrum. It is considered reliable due to the lack of characteristic lines in this region.

The results in Fig. 3 demonstrate that the photorecombination region of the spectrum between 3 and 4.8 Å is a featureless and relatively bright region, making it a suitable XRS for absorption spectroscopy. This is consistent with our earlier conclusions in Sec. II, which were based on an analysis of the model spectra shown in Fig. 1.

The XRS emissivity or yield depends on the target configuration. Figure 4 shows how this depends on target thickness and whether the target is uncoated or coated by a plastic layer. It shows the emissivity of the targets of different thickness in terms of the conversion efficiency, i.e., the full energy of the photons emitted by the plasma into 4π (assuming isotropic emission), in a given spectral bandwidth, normalized by the laser energy incident on the target. The spectra were integrated over the 0.5-Å spectral region where the photorecombination continuum intensity is a maximum. This was 4.5 Å–5 Å and 5.15 Å–5.65 Å for silicon and aluminum, respectively. The relative emissivity and associated errors were determined from several shots for a fixed target thickness and similar laser parameters.

The data clearly reveal that there is an optimal target thickness of around 10 μm for both silicon and aluminum. For thinner targets, the

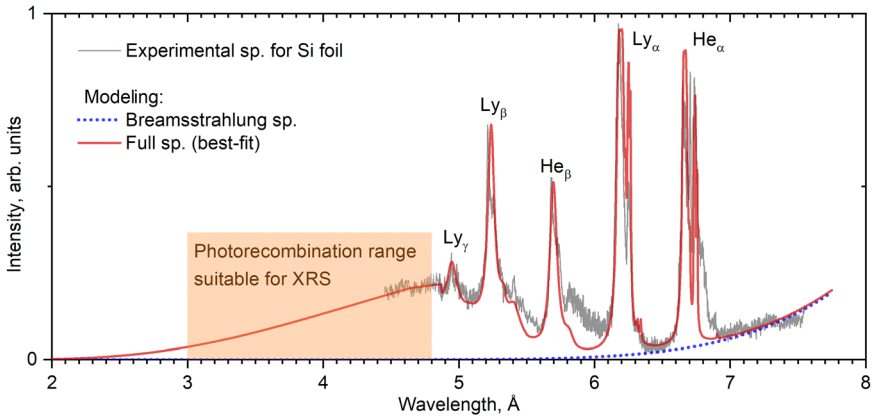

FIG. 3. Comparison of experimental data (grey curve) with a model spectrum (red curve). The experimental spectrum corresponds to 2-μm-Si-foil laser-plasma emission. The modeled spectrum is a sum of photorecombination, characteristic, and bremsstrahlung spectra; the last of these is indicated with a dotted blue curve. The orange rectangle indicates the wavelength range that is best suited for X-ray source based on Si (3 Å–4.8 Å).

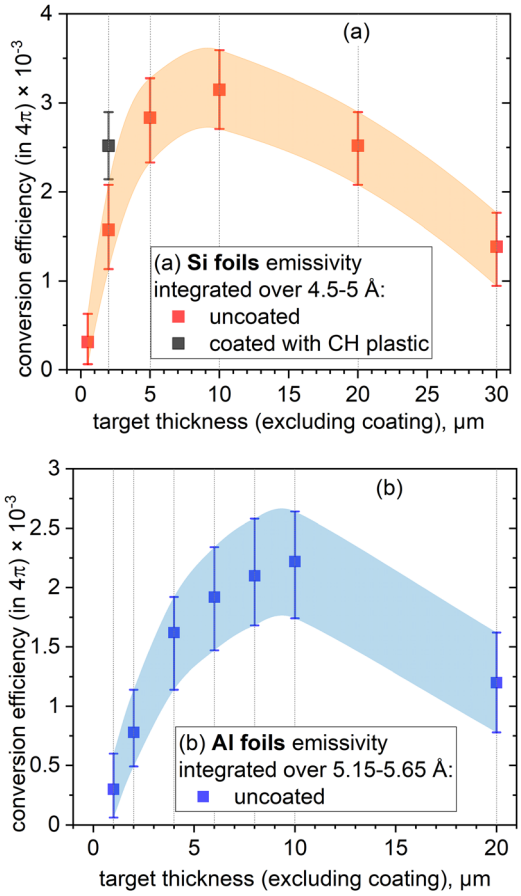

FIG. 4. Dependences of experimentally measured conversion efficiencies on the thickness of solid foil targets: (a) emission from silicon targets integrated over the wavelength range 4.5 Å–5 Å and (b) emission from aluminum targets integrated over the range 5.15 Å–5.65 Å. The conversion efficiency is the ratio of the deposited laser energy and the energy of the emitted photons.

decrease in emissivity is the result of a residual prepulse, which causes the target to expand. The decrease in plasma density reduces the recombination rate, so the X-ray yield drops, making thin targets unsuitable for XRS. When the target thickness was increased to 10 μm, the influence of the laser prepulse on the average plasma density reduced. A further increase in target thickness reduces the emissivity due to two factors. First, for a thicker target, the lowest electric potential is at the back surface of the target, which limits the refluxing of return currents of free electrons, reduces resistive heating, and reduces the target temperature. Second, the opacity of a thicker target reduces the emission from inner and rear layers.

The advantage of using plastic-coated targets to bury the emission layer is highlighted by the data point indicated by a black square in Fig. 4(a). The integrated emissivity is higher than for uncoated targets of the same thickness. Such a plastic coating is transparent to the laser pulses and suppresses expansion of the emission layer until the main laser pulse arrives. This helps to maintain a high average plasma density. In addition, the ionization potential depression extends the photorecombination continuum along the spectral range, which is described in more detail in Ref. 56. Though we studied coating only a 2-μm-thick foil, we expect similar emissivity enhancements for thicker targets.

IV. CONCLUSIONS

In this work, we discussed choosing a material and configuration of a solid target for use as a bright laser-plasma-based X-ray source. We show that low-Z materials, such as aluminum and silicon, can be used as X-ray backlighting in a hard X-ray range between 2 Å and 6 Å, which corresponds to photon energies of approximately 2 keV–6 keV. We focused on the photorecombination continuum emission of a solid-density plasma to create a featureless spectral continuum of high intensity, for use in, for example, XAS of WDM.

We studied experimentally spectrally resolved emissions from aluminum and silicon solid targets. We found that it is essential to use a high-contrast, high-intensity, and short-duration laser to create the X-ray sources and that an optimal target thickness of close to 10 μm is necessary. The lower emissivity of thinner targets, even with a high-contrast plasma pulse, is due to target expansion and a lowering of the average plasma density. A decrease of the emissivity for thicker targets is associated with a reduction of electron refluxing, resistive heating, and target opacity. A thin plastic coating on the target surface, which is transparent to the early part of a high-contrast laser pulse, helps to maintain the average plasma density and improve the X-ray emissivity.

The maximum number of the photons occurs for a 10-μm-thick Si foil and is about 10^{13} (assuming isotropic emission into 4π). However, when making XRS measurements during a specific high-power laser experiment, this value will likely decrease. The energy deposited into the main target usually exceeds that deposited into the XRS target. However, the plasma luminosity is directly proportional to the deposited laser energy. Therefore, the total main target luminosity is likely to be higher than the XRS one. Successful absorption spectroscopy seems to be impossible to perform in such conditions when recording photons emitted by both targets, as the signal-to-noise ratio is too high. However, most of the plasma emission comes from the hot laser–target interaction point and its surroundings, mainly as He-like characteristic emission lines. In a recent experimental campaign,[69] it was shown that the hot plasma emission is at least one order of magnitude higher than the WDM emission in the K-edge region. The temperature of the WDM was about a few tens of eV. This means that one should ensure proper shielding of the hot plasma emission from the main target (without decreasing the useful XRS signal). In this case, adsorption spectroscopy is possible. In general, an acceptable adsorption spectroscopy signal-to-noise ratio may be attained when the laser energy deposited in the XRS target is no less than 5 times lower than that deposited in the main target.

ACKNOWLEDGMENTS

The study was supported financially by the Russian Foundation for Basic Research (Grant No. 20-02-00790) and as a state assignment by the Joint Institute for High Temperatures of the Russian Academy of Sciences (Topic Grant No. 01201357846). The UK team received financial support from the Engineering and Physical Sciences Research Council (Grant Nos. EP/L01663X/1 and EP/H012605/1).

REFERENCES

[1]O. Renner and F. B. Rosmej, "Challenges of X-ray spectroscopy in investigations of matter under extreme conditions," Matter Radiat. Extremes **4**, 024201 (2019).

[2]I. Y. Skobelev, S. N. Ryazantsev, D. D. Arich, P. S. Bratchenko, A. Y. Faenov, T. A. Pikuz, P. Durey, L. Doehl, D. Farley, C. D. Baird, K. L. Lancaster, C. D. Murphy, N. Booth, C. Spindloe, P. McKenna, S. B. Hansen, J. Colgan, R. Kodama, N. Woolsey, and S. A. Pikuz, "X-ray absorption spectroscopy study of energy transport in foil targets heated by petawatt laser pulses," Photonics Res. **6**, 234 (2018).

[3]E. D. Filippov, I. Y. Skobelev, G. Revet, S. N. Chen, B. Khiar, A. Ciardi, D. Khaghani, D. P. Higginson, S. A. Pikuz, and J. Fuchs, "X-ray spectroscopy evidence for plasma shell formation in experiments modeling accretion columns in young stars," Matter Radiat. Extremes **4**, 064402 (2019).

[4]C. Bressler and M. Chergui, "Ultrafast X-ray absorption spectroscopy," Chem. Rev. **104**, 1781–1812 (2004).

[5]S. Tzortzakis, P. Audebert, P. Renaudin, S. Bastiani-Ceccotti, J. P. Geindre, C. Chenais-Popovics, V. Nagels, S. Gary, R. Shepherd, F. Girard, I. Matsushima, O. Peyrusse, and J. C. Gauthier, "Time- and space-resolved X-ray absorption spectroscopy of aluminum irradiated by a subpicosecond high-power laser," J. Quant. Spectrosc. Radiat. Transfer **99**, 614 (2006).

[6]P. Audebert, P. Renaudin, S. Bastiani-Ceccotti, J.-P. Geindre, C. Chenais-Popovics, S. Tzortzakis, V. Nagels-Silvert, R. Shepherd, I. Matsushima, S. Gary, F. Girard, O. Peyrusse, and J.-C. Gauthier, "Picosecond time-resolved X-ray absorption spectroscopy of ultrafast aluminum plasmas," Phys. Rev. Lett. **94**, 025004 (2005).

[7]R. W. Eason, D. K. Bradley, J. D. Kilkenny, and G. N. Greaves, "Improved laser-EXAFS studies of aluminium foil," J. Phys. C: Solid State Phys. **17**, 5067–5074 (1984).

[8]B. A. Remington, R. E. Rudd, and J. S. Wark, "From microjoules to megajoules and kilobars to gigabars: Probing matter at extreme states of deformation," Phys. Plasmas. **22**, 090501 (2015).

[9]H. Sawada, S. P. Regan, P. B. Radha, R. Epstein, D. Li, V. N. Goncharov, S. X. Hu, D. D. Meyerhofer, J. A. Delettrez, P. A. Jaanimagi, V. A. Smalyuk, T. R. Boehly, T. C. Sangster, B. Yaakobi, and R. C. Mancini, "Al 1s-2p absorption spectroscopy of shock-wave heating and compression in laser-driven planar foil," Phys. Plasmas **16**, 052702 (2009).

[10]M. Harmand, A. Ravasio, S. Mazevet, J. Bouchet, A. Denoeud, F. Dorchies, Y. Feng, C. Fourment, E. Galtier, J. Gaudin, F. Guyot, R. Kodama, M. Koenig, H. J. Lee, K. Miyanishi, G. Morard, R. Musella, B. Nagler, M. Nakatsutsumi, N. Ozaki, V. Recoules, S. Toleikis, T. Vinci, U. Zastrau, D. Zhu, and A. Benuzzi-Mounaix, "X-ray absorption spectroscopy of iron at multimegabar pressures in laser shock experiments," Phys. Rev. B. **92**, 024108 (2015).

[11]Y. Ping, F. Coppari, D. G. Hicks, B. Yaakobi, D. E. Fratanduono, S. Hamel, J. H. Eggert, J. R. Rygg, R. F. Smith, D. C. Swift, D. G. Braun, T. R. Boehly, and G. W. Collins, "Solid iron compressed up to 560 GPa," Phys. Rev. Lett. **111**, 065501 (2013).

[12]B. Yaakobi, T. R. Boehly, D. D. Meyerhofer, T. J. B. Collins, B. A. Remington, P. G. Allen, S. M. Pollaine, H. E. Lorenzana, and J. H. Eggert, "EXAFS measurement of iron bcc-to-hcp phase transformation in nanosecond-laser shocks," Phys. Rev. Lett. **95**, 075501 (2005).

[13]T. A. Hall, A. Djaoui, R. W. Eason, C. L. Jackson, B. Shiwai, S. L. Rose, A. Cole, and P. Apte, "Experimental observation of ion correlation in a dense laser-produced plasma," Phys. Rev. Lett. **60**, 2034–2037 (1988).

[14]M. E. Foord, R. F. Heeter, H.-K. Chung, P. A. M. van Hoof, J. E. Bailey, M. E. Cuneo, D. A. Liedahl, K. B. Fournier, V. Jonauskas, R. Kisielius, C. Ramsbottom, P. T. Springer, F. P. Keenan, S. J. Rose, and W. H. Goldstein, "Study of X-ray photoionized Fe plasma and comparisons with astrophysical modeling codes," J. Quant. Spectrosc. Radiat. Transfer **99**, 712–729 (2006).

[15]J. J. MacFarlane, J. E. Bailey, G. A. Chandler, C. Deeney, M. R. Douglas, D. Jobe, P. Lake, T. J. Nash, D. S. Nielsen, R. B. Spielman, P. Wang, and P. Woodruff, "X-ray absorption spectroscopy measurements of thin foil heating by Z -pinch radiation," Phys. Rev. E. **66**, 046416 (2002).

[16]J. Zhang, H. Li, Y. Zhao, G. Xiong, Z. Yuan, H. Zhang, G. Yang, J. Yang, S. Liu, S. Jiang, Y. Ding, B. Zhang, Z. Zheng, Y. Xu, X. Meng, and J. Yan, "L- and M-shell absorption measurements of radiatively heated Fe plasma," Phys. Plasmas. **19**, 113302 (2012).

[17]K. Falk, "Experimental methods for warm dense matter research," High Power Laser Sci. Eng. **6**, e59 (2018).

[18]A. Lévy, F. Dorchies, M. Harmand, C. Fourment, S. Hulin, O. Peyrusse, J. J. Santos, P. Antici, P. Audebert, J. Fuchs, L. Lancia, A. Mancic, M. Nakatsutsumi, S. Mazevet, V. Recoules, P. Renaudin, and S. Fourmaux, "X-ray absorption for the study of warm dense matter," Plasma Phys. Control. Fusion. **51**, 124021 (2009).

[19]B. I. Cho, K. Engelhorn, A. A. Correa, T. Ogitsu, C. P. Weber, H. J. Lee, J. Feng, P. A. Ni, Y. Ping, A. J. Nelson, D. Prendergast, R. W. Lee, R. W. Falcone, and P. A. Heimann, "Electronic structure of warm dense copper studied by ultrafast x-ray absorption spectroscopy," Phys. Rev. Lett. **106**, 167601 (2011).

[20]F. Dorchies, V. Recoules, J. Bouchet, C. Fourment, P. M. Leguay, B. I. Cho, K. Engelhorn, M. Nakatsutsumi, C. Ozkan, T. Tschentscher, M. Harmand, S. Toleikis, M. Störmer, E. Galtier, H. J. Lee, B. Nagler, P. A. Heimann, and J. Gaudin, "Time evolution of electron structure in femtosecond heated warm dense molybdenum," Phys. Rev. B. **92**, 144201 (2015).

[21]R. Betti and O. A. Hurricane, "Inertial-confinement fusion with lasers," Nat. Phys. **12**, 435–448 (2016).

[22]D. Batani, S. Baton, A. Casner, S. Depierreux, M. Hohenberger, O. Klimo, M. Koenig, C. Labaune, X. Ribeyre, C. Rousseaux, G. Schurtz, W. Theobald, and V. T. Tikhonchuk, "Physics issues for shock ignition," Nucl. Fusion. **54**, 054009 (2014).

[23]J. E. Bailey, T. Nagayama, G. P. Loisel, G. A. Rochau, C. Blancard, J. Colgan, P. Cosse, G. Faussurier, C. J. Fontes, F. Gilleron, I. Golovkin, S. B. Hansen, C. A. Iglesias, D. P. Kilcrease, J. J. MacFarlane, R. C. Mancini, S. N. Nahar, C. Orban, J.-C. Pain, A. K. Pradhan, M. Sherrill, and B. G. Wilson, "A higher-than-predicted measurement of iron opacity at solar interior temperatures," Nature **517**, 56–59 (2015).

[24]S. N. Nahar and A. K. Pradhan, "Large enhancement in high-energy photoionization of Fe XVII and missing continuum plasma opacity," Phys. Rev. Lett. **116**, 235003 (2016).

[25]L. Miaja-Avila, G. C. O'Neil, J. Uhlig, C. L. Cromer, M. L. Dowell, R. Jimenez, A. S. Hoover, K. L. Silverman, and J. N. Ullom, "Laser plasma x-ray source for ultrafast time-resolved x-ray absorption spectroscopy," Struct. Dyn. **2**, 024301 (2015).

[26]M. V. Sedov, A. Y. Faenov, A. A. Andreev, I. Y. Skobelev, S. N. Ryazantsev, T. A. Pikuz, P. Durey, L. Doehl, D. Farley, C. D. Baird, K. L. Lancaster, C. D. Murphy, N. Booth, C. Spindloe, K. Y. Platonov, P. McKenna, R. Kodama, N. Woolsey, and S. A. Pikuz, "Features of the generation of fast particles from microstructured targets irradiated by high intensity, picosecond laser pulses," Laser Part. Beams **37**, 176–183 (2019).

[27]M. A. Alkhimova, A. Y. Faenov, I. Y. Skobelev, T. A. Pikuz, M. Nishiuchi, H. Sakaki, A. S. Pirozhkov, A. Sagisaka, N. P. Dover, K. Kondo, K. Ogura, Y. Fukuda, H. Kiriyama, K. Nishitani, T. Miyahara, Y. Watanabe, S. A. Pikuz, M. Kando, R. Kodama, and K. Kondo, "High resolution X-ray spectra of stainless steel foils irradiated by femtosecond laser pulses with ultra-relativistic intensities," Opt. Express. **25**, 29501 (2017).

[28]V. V. Gavrilov, A. G. Es'kov, A. M. Zhitlukhin, D. M. Kochnev, S. A. Pikuz, I. M. Poznyak, S. N. Ryazantsev, I. Y. Skobelev, D. A. Toporkov, and N. M. Umrikhin, "High-power X-ray line radiation of the plasma produced in a collision of high-energy plasma flows," Plasma Phys. Rep. **44**, 820 (2018).

[29]F. Dorchies, A. Lévy, C. Goyon, P. Combis, D. Descamps, C. Fourment, M. Harmand, S. Hulin, P. M. Leguay, S. Petit, O. Peyrusse, and J. J. Santos, "Unraveling the solid-liquid-vapor phase transition dynamics at the atomic level with ultrafast x-ray absorption near-edge spectroscopy," Phys. Rev. Lett. **107**, 245006 (2011).

[30]F. Dorchies and V. Recoules, "Non-equilibrium solid-to-plasma transition dynamics using XANES diagnostic," Phys. Rep. **657**, 1–26 (2016).

[31]S. Fourmaux, L. Lecherbourg, M. Harmand, M. Servol, and J. C. Kieffer, "High repetition rate laser produced soft x-ray source for ultrafast x-ray absorption near edge structure measurements," Rev. Sci. Instrum. **78**, 113104 (2007).

[32]A. D. Cahill, C. L. Hoyt, S. A. Pikuz, T. Shelkovenko, and D. A. Hammer, "A doubly curved elliptical crystal spectrometer for the study of localized x-ray absorption in hot plasmas," Rev. Sci. Instrum. **85**, 103114 (2014).

[33]T. A. Shelkovenko, S. A. Pikuz, and D. A. Hammer, "A review of projection radiography of plasma and biological objects in X-Pinch radiation," Plasma Phys. Rep. **42**, 226–268 (2016).

[34]D. P. Bernstein, Y. Acremann, A. Scherz, M. Burkhardt, J. Stöhr, M. Beye, W. F. Schlotter, T. Beeck, F. Sorgenfrei, A. Pietzsch, W. Wurth, and A. Föhlisch, "Near

edge x-ray absorption fine structure spectroscopy with x-ray free-electron lasers," Appl. Phys. Lett. **95**, 134102 (2009).

[35]M. Šmíd, I. Gallardo González, H. Ekerfelt, J. Björklund Svensson, M. Hansson, J. C. Wood, A. Persson, S. P. D. Mangles, O. Lundh, and K. Falk, "Highly efficient angularly resolving x-ray spectrometer optimized for absorption measurements with collimated sources," Rev. Sci. Instrum. **88**, 063102 (2017).

[36]B. Mahieu, N. Jourdain, K. Ta Phuoc, F. Dorchies, J.-P. Goddet, A. Lifschitz, P. Renaudin, and L. Lecherbourg, "Probing warm dense matter using femtosecond X-ray absorption spectroscopy with a laser-produced betatron source," Nat. Commun. **9**, 3276 (2018).

[37]B. Kettle, E. Gerstmayr, M. J. V. Streeter, F. Albert, R. A. Baggott, N. Bourgeois, J. M. Cole, S. Dann, K. Falk, I. Gallardo González, A. E. Hussein, N. Lemos, N. C. Lopes, O. Lundh, Y. Ma, S. J. Rose, C. Spindloe, D. R. Symes, M. Šmíd, A. G. R. Thomas, R. Watt, and S. P. D. Mangles, "Single-shot multi-keV x-ray absorption spectroscopy using an ultrashort laser-wakefield accelerator source," Phys. Rev. Lett. **123**, 254801 (2019).

[38]N. Lemos, P. King, J. L. Shaw, A. L. Milder, K. A. Marsh, A. Pak, B. B. Pollock, C. Goyon, W. Schumaker, A. M. Saunders, D. Papp, R. Polanek, J. E. Ralph, J. Park, R. Tommasini, G. J. Williams, H. Chen, F. V. Hartemann, S. Q. Wu, S. H. Glenzer, B. M. Hegelich, J. Moody, P. Michel, C. Joshi, and F. Albert, "X-ray sources using a picosecond laser driven plasma accelerator," Phys. Plasmas. **26**, 083110 (2019).

[39]M. Z. Mo, Z. Chen, S. Fourmaux, A. Saraf, S. Kerr, K. Otani, R. Masoud, J.-C. Kieffer, Y. Tsui, A. Ng, and R. Fedosejevs, "Measurements of ionization states in warm dense aluminum with betatron radiation," Phys. Rev. E. **95**, 053208 (2017).

[40]I. Mantouvalou, A. Jonas, K. Witte, R. Jung, H. Stiel, and B. Kanngießer, "Optimizing soft X-ray NEXAFS spectroscopy in the laboratory," Proc. SPIE **10243**, 1024308 (2017).

[41]G. Loisel, P. Arnault, S. Bastiani-Ceccotti, T. Blenski, T. Caillaud, J. Fariaut, W. Fölsner, F. Gilleron, J.-C. Pain, M. Poirier, C. Reverdin, V. Silvert, F. Thais, S. Turck-Chièze, and B. Villette, "Absorption spectroscopy of mid and neighboring Z plasmas: Iron, nickel,copper and germanium," High Energy Density Phys. **5**, 173–181 (2009).

[42]P. J. Mallozzi, R. E. Schwerzel, H. M. Epstein, and B. E. Campbell, "Laser-EXAFS: Fast extended x-ray absorption fine structure spectroscopy with a single pulse of laser-produced x-rays," Science **206**, 353–355 (1979).

[43]P. Wachulak, T. Fok, A. Bartnik, K. A. Janulewicz, and H. Fiedorowicz, "EXAFS of titanium L_{III} edge using a compact laboratory system based on a laser-plasma soft X-ray source," Appl. Phys. B. **126**, 11 (2020).

[44]A. Krygier, F. Coppari, G. E. Kemp, D. B. Thorn, R. S. Craxton, J. H. Eggert, E. M. Garcia, J. M. McNaney, H.-S. Park, Y. Ping, B. A. Remington, and M. B. Schneider, "Developing a high-flux, high-energy continuum backlighter for extended x-ray absorption fine structure measurements at the National Ignition Facility," Rev. Sci. Instrum. **89**, 10F114 (2018).

[45]Y. Hu, S. Jiang, J. Zhang, Q. Xue, Z. Wang, and Q. Ye, "X-ray source improvements for EXAFS measurement on SGIII prototype facility," AIP Adv. **10**, 055313 (2020).

[46]B. Yaakobi, F. J. Marshall, T. R. Boehly, R. P. J. Town, and D. D. Meyerhofer, "Extended x-ray absorption fine-structure experiments with a laser-imploded target as a radiation source," J. Opt. Soc. Am. B. **20**, 238 (2003).

[47]J. H. Sung, H. W. Lee, J. Y. Yoo, J. W. Yoon, C. W. Lee, J. M. Yang, Y. J. Son, Y. H. Jang, S. K. Lee, and C. H. Nam, "42 PW, 20 fs Ti:sapphire laser at 01 Hz," Opt. Lett. **42**, 2058 (2017).

[48]S. Gales, K. A. Tanaka, D. L. Balabanski, F. Negoita, D. Stutman, O. Tesileanu, C. A. Ur, D. Ursescu, I. Andrei, S. Ataman, M. O. Cernaianu, L. D'Alessi, I. Dancus, B. Diaconescu, N. Djourelov, D. Filipescu, P. Ghenuche, D. G. Ghita, C. Matei, K. Seto, M. Zeng, and N. V. Zamfir, "The extreme light infrastructure—Nuclear physics (ELI-NP) facility: New horizons in physics with 10 PW ultra-intense lasers and 20 MeV brilliant gamma beams," Rep. Prog. Phys. **81**, 094301 (2018).

[49]D. N. Papadopoulos, P. Ramirez, K. Genevrier, L. Ranc, N. Lebas, A. Pellegrina, C. Le Blanc, P. Monot, L. Martin, J. P. Zou, F. Mathieu, P. Audebert, P. Georges, and F. Druon, "High-contrast 10 fs OPCPA-based front end for multi-PW laser chains," Opt. Lett. **42**, 3530 (2017).

[50]L. Yu, Y. Xu, Y. Liu, Y. Li, S. Li, Z. Liu, W. Li, F. Wu, X. Yang, Y. Yang, C. Wang, X. Lu, Y. Leng, R. Li, and Z. Xu, "High-contrast front end based on cascaded XPWG and femtosecond OPA for 10-PW-level Ti:sapphire laser," Opt. Express. **26**, 2625 (2018).

[51]H. Kiriyama, A. S. Pirozhkov, M. Nishiuchi, Y. Fukuda, K. Ogura, A. Sagisaka, Y. Miyasaka, M. Mori, H. Sakaki, N. P. Dover, K. Kondo, J. K. Koga, T. Z. Esirkepov, M. Kando, and K. Kondo, "High-contrast high-intensity repetitive petawatt laser," Opt. Lett. **43**, 2595 (2018).

[52]D. Riley, J. J. Angulo-Gareta, F. Y. Khattak, M. J. Lamb, P. S. Foster, E. J. Divall, C. J. Hooker, A. J. Langley, R. J. Clarke, and D. Neely, "Kα yields from Ti foils irradiated with ultrashort laser pulses," Phys. Rev. E. **71**, 016406 (2005).

[53]K. B. Wharton, C. D. Boley, A. M. Komashko, A. M. Rubenchik, J. Zweiback, J. Crane, G. Hays, T. E. Cowan, and T. Ditmire, "Effects of nonionizing prepulses in high-intensity laser-solid interactions," Phys. Rev. E. **64**, 025401 (2001).

[54]A. L. Kritcher, P. Neumayer, M. K. Urry, H. Robey, C. Niemann, O. L. Landen, E. Morse, and S. H. Glenzer, "K-alpha conversion efficiency measurements for X-ray scattering in inertial confinement fusion plasmas," High Energy Density Phys. **3**, 156–162 (2007).

[55]S. N. Chen, G. Gregori, P. K. Patel, H.-K. Chung, R. G. Evans, R. R. Freeman, E. Garcia Saiz, S. H. Glenzer, S. B. Hansen, F. Y. Khattak, J. A. King, A. J. Mackinnon, M. M. Notley, J. R. Pasley, D. Riley, R. B. Stephens, R. L. Weber, S. C. Wilks, and F. N. Beg, "Creation of hot dense matter in short-pulse laser-plasma interaction with tamped titanium foils," Phys. Plasmas. **14**, 102701 (2007).

[56]A. S. Martynenko, S. A. Pikuz, I. Y. Skobelev, S. N. Ryazantsev, C. Baird, N. Booth, L. Doehl, P. Durey, A. Y. Faenov, D. Farley, R. Kodama, K. Lancaster, P. McKenna, C. D. Murphy, C. Spindloe, T. A. Pikuz, and N. Woolsey, "Effect of plastic coating on the density of plasma formed in Si foil targets irradiated by ultra-high-contrast relativistic laser pulses," Phys. Rev. E. **101**, 043208 (2020).

[57]J. J. MacFarlane, I. E. Golovkin, P. R. Woodruff, D. R. Welch, B. V. Oliver, T. A. Mehlhorn, and R. B. Campbell, "Simulation of the ionization dynamics of aluminum irradiated by intense short-pulse lasers," in *Inertial Fusion Sciences and Applications 2003* (American Nuclear Society, 2004), p. 457.

[58]J. J. MacFarlane, I. E. Golovkin, P. Wang, P. R. Woodruff, and N. A. Pereyra, "SPECT3D—A multi-dimensional collisional-radiative code for generating diagnostic signatures based on hydrodynamics and PIC simulation output," High Energy Density Phys. **3**, 181 (2007).

[59]D. J. Hoarty, P. Allan, S. F. James, C. R. D. Brown, L. M. R. Hobbs, M. P. Hill, J. W. O. Harris, J. Morton, M. G. Brookes, R. Shepherd, J. Dunn, H. Chen, E. Von Marley, P. Beiersdorfer, H. K. Chung, R. W. Lee, G. Brown, and J. Emig, "Observations of the effect of ionization-potential depression in hot dense plasma," Phys. Rev. Lett. **110**, 265003 (2013).

[60]O. Ciricosta, S. M. Vinko, B. Barbrel, D. S. Rackstraw, T. R. Preston, T. Burian, J. Chalupský, B. I. Cho, H. K. Chung, G. L. Dakovski, K. Engelhorn, V. Hájková, P. Heimann, M. Holmes, L. Juha, J. Krzywinski, R. W. Lee, S. Toleikis, J. J. Turner, U. Zastrau, and J. S. Wark, "Measurements of continuum lowering in solid-density plasmas created from elements and compounds," Nat. Commun. **7**, 11713 (2016).

[61]D. G. Hummer and D. Mihalas, "The equation of state for stellar envelopes. I. An occupation probability formalism for the truncation of internal partition functions," Astrophys. J. **331**, 794 (1988).

[62]C. N. Danson, P. A. Brummitt, R. J. Clarke, J. L. Collier, B. Fell, A. J. Frackiewicz, S. Hancock, S. Hawkes, C. Hernandez-Gomez, P. Holligan, M. H. R. Hutchinson, A. Kidd, W. J. Lester, I. O. Musgrave, D. Neely, D. R. Neville, P. A. Norreys, D. A. Pepler, C. J. Reason, W. Shaikh, T. B. Winstone, R. W. W. Wyatt, and B. E. Wyborn, "Vulcan petawatt—An ultra-high-intensity interaction facility," Nucl. Fusion **44**, S239–S246 (2004).

[63]G. A. Mourou, T. Tajima, and S. V. Bulanov, "Optics in the relativistic regime," Rev. Mod. Phys. **78**, 309–371 (2006).

[64]G. Doumy, F. Quéré, O. Gobert, M. Perdrix, P. Martin, P. Audebert, J. C. Gauthier, J.-P. Geindre, and T. Wittmann, "Complete characterization of a plasma mirror for the production of high-contrast ultraintense laser pulses," Phys. Rev. E. **69**, 026402 (2004).

[65]R. Hörlein, B. Dromey, D. Adams, Y. Nomura, S. Kar, K. Markey, P. Foster, D. Neely, F. Krausz, G. D. Tsakiris, and M. Zepf, "High contrast plasma mirror: Spatial

filtering and second harmonic generation at 10^{19} W cm^{-2}," New J. Phys. **10**, 083002 (2008).

[66]C. Hernandez-Gomez, "Overview of the central laser facility (CLF)," CLF Annual Reports No. 2016-2017, 2017, pp. 6–8.

[67]A. Y. Faenov, S. A. Pikuz, A. I. Erko, B. A. Bryunetkin, V. M. Dyakin, G. V. Ivanenkov, A. R. Mingaleev, T. A. Pikuz, V. M. Romanova, and T. A. Shelkovenko, "High-performance x-ray spectroscopic devices for plasma microsources investigations," Phys. Scr. **50**, 333–338 (1994).

[68]M. A. Alkhimova, I. Y. Skobelev, A. Y. Faenov, D. A. Arich, T. A. Pikuz, and S. A. Pikuz, "Accounting for the instrument function of crystal spectrometers operating in many reflection orders in the diagnostics of laser plasma from its continuum spectrum," Quantum Electron. **48**, 749–754 (2018).

[69]A. Schönlein, G. Boutoux, S. Pikuz, L. Antonelli, D. Batani, A. Debayle, A. Franz, L. Giuffrida, J. J. Honrubia, J. Jacoby, D. Khaghani, P. Neumayer, O. N. Rosmej, T. Sakaki, J. J. Santos, and A. Sauteray, "Generation and characterization of warm dense matter isochorically heated by laser-induced relativistic electrons in a wire target," EPL (Europhys. Lett.) **114**, 45002 (2016).